Available online at www.sciencedirect.com
SCIENCE DIRECT®
International Journal of Thermal Sciences 44 (2005) 277–288
International Journal of Thermal Sciences
www.elsevier.com/locate/ijts

Ammonia–water absorption in vertical tubular absorbers

José Fernández-Seara *, Jaime Sieres, Cristóbal Rodríguez, Manuel Vázquez

Área de Máquinas y Motores Térmicos, Escuela Técnica Superior de Ingenieros Industriales, Campus Lagoas-Marcosende, Nº 9, 36200 Vigo, Spain

Received 15 March 2004; received in revised form 13 July 2004; accepted 20 September 2004

Available online 21 November 2004

Abstract

This paper presents a detailed analysis of the heat and mass transfer processes during the absorption of ammonia into water in a co-current vertical tubular absorber. The absorber configuration is of the shell and tubes type. The absorption process progresses as the vapour and liquid contact inside the tubes. Water is used as the absorber cooling medium. A differential mathematical model has been developed on the basis of mass and energy balances and heat and mass transfer equations, in order to provide further understanding of the absorber behaviour. The model takes into account separately for the churn, slug and bubbly flow patterns experimentally forecasted in this type of absorption processes inside vertical tubes and considers the simultaneous heat and mass transfer processes in both liquid and vapour phases, as well as heat transfer to the cooling medium. The model equations have been solved using the finite-difference method. Results obtained for specific data are depicted to show local values of the most important variables all along the absorber length. Parametric analyses have been performed to show the influence of design parameters and operating conditions on the absorber performance. The effect of the heat and mass transfer coefficients has also been evaluated.

Keywords: Vertical tubular absorber; Ammonia–water; Absorption refrigeration; Heat transfer; Mass transfer; Flow patterns

1. Introduction

Intensive research has been developed in the absorption technology since its last revival in the 1970s. However the technological solutions available are not completely successful, especially in the branch of small size machines powered with residual and/or renewal energies [1]. The binary mixture ammonia-water is the most common working pair used in this technology since its beginnings and nowadays there is no doubt that prevails with a clear future [2]. Moreover the specific properties of this mixture offer the possibility of using different types of cycles and components whose design need to be carefully analysed and evaluated [3]. Mainly, the components used for the absorption and the generation-purification processes should be selected and designed carefully [4–6].

The absorber design has a decisive importance on the absorption system since not only the cycle performance depends on its design but also the system cost. The simultaneous heat and mass transfer mechanisms occurring in the absorber have been widely researched, especially in the last three decades. The complex and coupled interaction between heat and mass transfer complicates the study of the absorption process since the conditions that establish the transport phenomena change as the process progresses. Moreover, the hydrodynamics in the absorber plays an important role on its performance; therefore the knowledge of the two-phase flow behaviour is also needed.

Bubble-type absorbers were strongly recommended for ammonia-water absorption systems instead of the thin falling film mode because bubble-type provides high heat transfer coefficients and vapour distribution is easier than the liquid distribution needed in the falling film absorbers [7]. Several attempts to model, numerically and analytically, the heat and mass transfer processes in bubble absorbers can be found in the literature. Infante Ferreira et al. [8] devel-

* Corresponding author. Tel.: +34 986 812605, fax: +34 986 811995.
E-mail addresses: jseara@uvigo.es (J. Fernández-Seara), jsieres@uvigo.es (J. Sieres), mvazquez@uvigo.es (M. Vázquez).

1290-0729/$ – see front matter
doi:10.1016/j.ijthermalsci.2004.09.001

Nomenclature

A	transfer area	m^2
a_{esp}	specific interfacial area	$m^2 \cdot m^{-3}$
c	heat transfer correction factor	
c_p	specific heat	$J \cdot kg^{-1} \cdot K^{-1}$
$\tilde{c}_p$	partial mass specific heat	$J \cdot kg^{-1} \cdot K^{-1}$
d	tube diameter	m
F	mass transfer coefficient	$kmol \cdot m^{-2} \cdot s^{-1}$
h	specific enthalpy	$J \cdot kg^{-1}$
$\tilde{h}$	partial enthalpy	$J \cdot kg^{-1}$
i	element incremental number	
j	between-baffles section incremental number	
k_w	tube wall thermal conductivity	$W \cdot m^{-1} \cdot K^{-1}$
$\overline{M}$	molecular weight	$kg \cdot kmol^{-1}$
$\dot{M}$	mass flow	$kg \cdot s^{-1}$
$\dot{m}$	mass flux	$kg \cdot m^{-2} \cdot s^{-1}$
$\dot{N}_b$	Bubble frequency	s^{-1}
N_b	number of baffles	
N_t	number of tubes	
n	number of discrete elements	
$\dot{n}$	molar flux	$kmol \cdot m^{-2} \cdot s^{-1}$
n_{sb}	number of discrete elements between baffles	
r_i	interfacial radius	m
r_s	coolant side fouling factor	$m^2 \cdot K \cdot W^{-1}$
T	temperature	K
U_{out}	overall heat transfer coefficient	$W \cdot m^{-2} \cdot K^{-1}$
u_v	mean bubble rise velocity	$m \cdot s^{-1}$
V	total volume flux	$m \cdot s^{-1}$
V_{Lf}	mean velocity in the film	$m \cdot s^{-1}$
x	ammonia mass concentration	kg $NH_3 \cdot kg^{-1}$
$\bar{x}$	ammonia molar concentration	kmol $NH_3 \cdot$ kmol^{-1}
y	coordinate along the absorber	m
y_b	slug bubble length	m
y_L	separation distance between two Taylor bubbles	m
y_{Lmin}	minimum separation distance between two Taylor bubbles	m
z	ratio of ammonia to the total molar flux	

Greek symbols

α	heat transfer coefficient	$W \cdot m^{-2} \cdot K^{-1}$
ε_v	void fraction	
φ	heat flux	$W \cdot m^{-2}$

Subscripts

b	bulk
c	coolant
ci	coolant inlet to between-baffles section
co	coolant outlet from between-baffles section
i	interface
L	liquid
Lf	liquid film
Lsp	liquid single-phase
v	vapour
w	wall
wi	inner wall
wo	outer wall

oped a calculation model for vertical tubular absorbers using experimental mean overall heat and mass transfer coefficients all along the absorber length. Although this method is a good design tool, it does not allow obtaining local values for important parameters such as temperature and concentration. Merrill et al. [9] put forward a boundary-layer theory approach that provides accurate solutions for temperature and concentration fields in the absorber. Herbine and Pérez-Blanco [10] developed a model for the absorption process in an ammonia–water bubble absorber with a vertical tube, which yielded temperature and concentration profiles along the absorber. However the resistance to mass transfer inside the bubbles was neglected in the model. Potnis et al. [11] used the Colburn and Drew [12] equations to develop a computer program for an ammonia–water GAX component with a fluted helical coil geometry. Kang et al. [7] proposed a design model for a bubble absorber with plate heat exchangers to evaluate the heat and mass transfer resistances within both liquid and bubble and to find optimum design conditions for the absorber. Kang et al. [13] compared the falling film and bubble modes, concluding that in bubble type the local absorption is always higher, the mixing is better and heat transfer coefficients are higher than those in the falling film mode.

The vapour–liquid co-current absorption process inside vertical tubes is characterised by a changing two-phase flow pattern. Churn flow takes place directly after the tube inlet and is followed by a developed slug flow and finally by a bubbly flow until the vapour absorption is completed. Therefore the analysis of a vertical tubular absorber should take account of the transitions between the three different flow regimes and the particularities in the heat and mass transfer processes in each one of them.

Many authors have studied the hydrodynamics of vertical co-current two-phase flow [14–20] and the transitions between different regimens [15,16,21–24]. Experimental results on heat or mass transfer for specific flow regimens are also available, but most of them do not study simultaneous heat and mass transfer and are based on systems where either heat or mass transfer resistances are neglected [25–28].

Experimental research for bubble absorption in ammonia–water systems is scarce, Infante Ferreira [8] studied churn, slug and bubbly flow in a vertical absorber obtaining experimental global heat and mass transfer coefficients. Tere-

saka et al. [29] investigated the mechanism of gas absorption from a bubble during bubble growth. Kang et al. [30] developed a mass transfer correlation for NH_3–H_2O in bubble absorbers, distinguishing the processes of bubble growth and bubble disappearance in the bubble absorption. Lee et al. [31] studied the mass transfer process in bubble mode absorber of ammonia and water. Kim et al. [32] studied a counter-current slug flow absorber working with the ammonia–water mixture and they distinguished two flow patterns, frost (churn) flow and slug flow, and measured the local heat transfer rate varying several parameters. The same authors [33] also developed a data reduction model to obtain the local heat and mass transfer coefficients in the liquid side, from the experimental results. They found that the flow pattern has an important influence on the heat and mass transfer coefficients in the liquid side.

This paper presents a detailed analysis of ammonia–water absorption process in vertical tubular absorbers of the shell and tubes type using water as the coolant. The churn, slug and bubbly flow patterns are considered separately in the analysis as well as the heat and mass transfer processes in the liquid and vapour phases. The analysis has been carried out by developing a differential mathematical model. The model is based on the equations reported by Colburn and Drew [12] and employs local heat and mass transfer coefficients.

2. System description

A schematic diagram of the vertical tubular absorber is shown in Fig. 1. The absorber consists of a tube bundle in a shell (shell and tubes type heat exchanger).

The ammonia vapour and the weak ammonia–water liquid solution are distributed at the bottom of the absorber and circulate co-currently upwards within the tubes. The vapour enters at the bottom of the absorber and is distributed into the tubes through small diameter nozzles. The liquid phase (weak solution) is also introduced at the bottom of the absorber, going into the tubes through the free area between tubes and nozzles. The absorption process progresses as the vapour and liquid contact inside the tubes. The liquid solution obtained (strong solution) is removed at the top of the absorber. Water is considered as the absorber cooling medium. A set of baffles is arranged transverse to the tube bundle to drive the coolant and to yield stiffness to the absorber (Fig. 1). The water flows downwards, external and transverse to the tube bundle, driven by the baffles and counter-currently to the liquid–vapour mixture.

Fig. 2 shows the typical temperature and concentration profiles for the co-current absorption of the ammonia–water mixture.

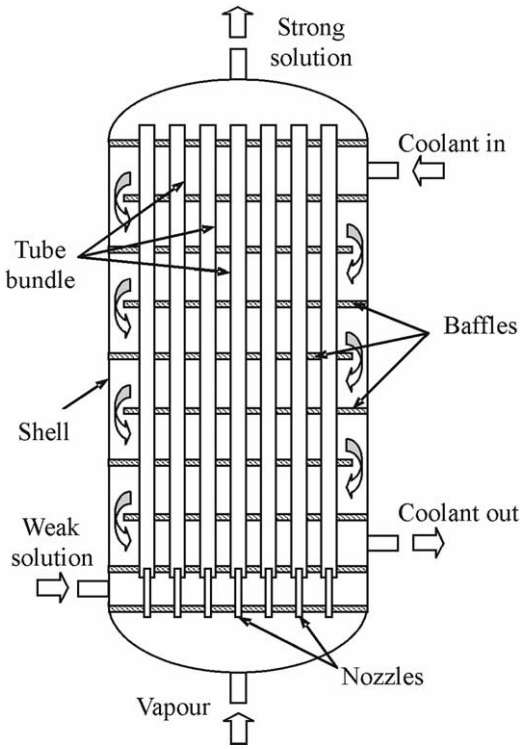

Fig. 1. Schematic diagram of the vertical tubular absorber.

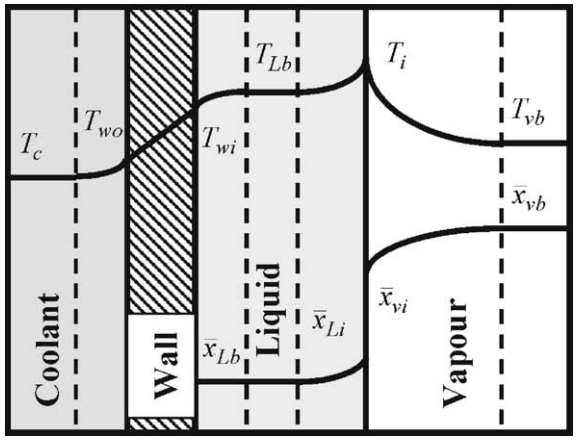

Fig. 2. Temperature and concentration profiles for the co-current absorption process.

3. Mathematical model

A differential mathematical model has been developed on the basis of mass and energy balances and heat and mass transfer equations. The model takes into account separately for the churn, slug and bubbly flow patterns and considers the simultaneous heat and mass transfer processes in both liquid and vapour phases, as well as heat transfer to the cooling water through the tube wall. In order to analyse the absorption process, mass, concentration and energy balances are considered, in the same way mass and heat transfer equations have been applied as well as the proper boundary conditions in a differential control volume. The differential

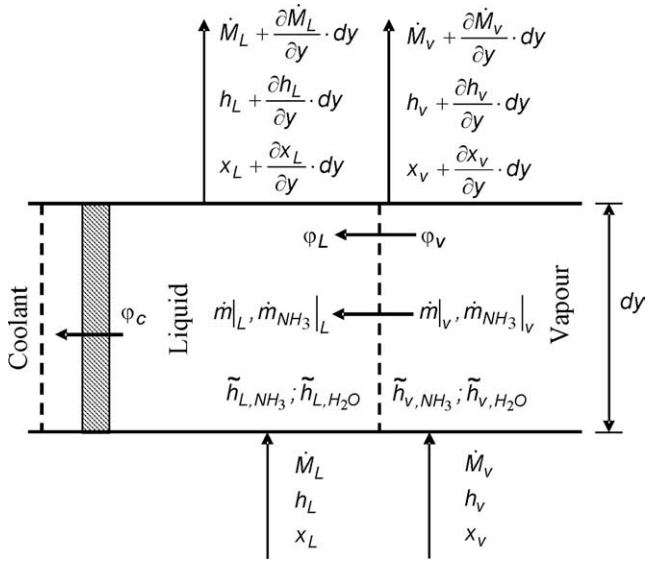

Fig. 3. Differential control volume.

control volume where the model equations are applied is depicted in Fig. 3.

The following assumptions have been made to develop the model.

(1) The absorption process is in steady state and the absorber pressure is constant.
(2) Heat losses to the environment are negligible.
(3) The two-film and the Lewis and Whitman theory [34] of non-interfacial resistance are applied, i.e., the interface concentrations of vapour and liquid are the equilibrium concentrations at the interface temperature.
(4) The heat and mass transfer areas between liquid and vapour phases are equal.
(5) Bubble coalescence and break-up are not considered.
(6) There is no direct heat transfer between the vapour and the coolant.
(7) For a transversal tube section, the coolant, liquid and vapour properties are assumed to be constant with the angular coordinate.

3.1. Mass transfer equations

Mass transfer between the vapour and the liquid phases results from the combined contribution of molecular diffusion (due to a concentration gradient) and a bulk transport of material through the interface [35–38].

The total molar flux $\dot{n}$ is the sum of ammonia $\dot{n}_{NH_3}$ and water $\dot{n}_{H_2O}$ molar fluxes, so the ratio of ammonia to the total molar flux (z) can be established according to Eq. (1).

$$z = \frac{\dot{n}_{NH_3}}{\dot{n}} \tag{1}$$

The molar flux of ammonia from the bulk vapour to the interface is obtained from Eq. (2) (see Fig. 2), where mass transfer is defined to be positive from the vapour to the interface.

$$\dot{n}_{NH_3}|_v = F_v z \,\mathrm{Ln}\left(\frac{z - \bar{x}_{vi}}{z - \bar{x}_{vb}}\right) \tag{2}$$

Likewise, the molar flux of ammonia from the interface to the bulk liquid is expressed in Eq. (3), where mass transfer is defined to be positive from the interface to the liquid phase.

$$\dot{n}_{NH_3}|_L = F_{Li} z \,\mathrm{Ln}\left(\frac{z - \bar{x}_{Lb}}{z - \bar{x}_{Li}}\right) \tag{3}$$

In order to carry out the mass continuity requirement at the interface, the mass transport in the liquid ($\dot{n}_{NH_3}|_L$) and vapour ($\dot{n}_{NH_3}|_v$) phases through the interface must be the same, as expressed in Eq. (4).

$$\dot{n}_{NH_3}|_L = \dot{n} z = \dot{n}_{NH_3}|_v \tag{4}$$

If the ammonia and total molar fluxes are determined, then the corresponding mass fluxes can be calculated from Eqs. (5) and (6), where $\overline{M}$ is the components' molecular weight.

$$\dot{m}_{NH_3} = \dot{n}_{NH_3} \overline{M}_{NH_3} \tag{5}$$

$$\dot{m} = \dot{n}_{NH_3} \overline{M}_{NH_3} + \dot{n}(1 - z)\overline{M}_{H_2O} \tag{6}$$

3.2. Heat transfer equations

There are two different regions in which heat transfer takes place, on the one hand the heat transfer between the vapour and the liquid phases, on the other hand the heat transfer between the liquid phase and the coolant through the tube wall.

Combined heat and mass transfer takes place in the liquid and vapour phases. Therefore, there is a sensible heat of the mass flux between the bulk and the interface conditions, which must be considered in the heat transfer equations. A detailed discussion of these equations can be found in the literature [35–37]. The sensible heat transferred from the bulk vapour to the interface (see Fig. 2) is given in Eq. (7). Heat transfer is defined to be positive from the vapour to the liquid phase.

$$\varphi_v = \alpha_v \frac{c_v}{1 - e^{-c_v}}(T_{vb} - T_i) \tag{7}$$

The sensible heat transferred from the interface to the bulk liquid is given by Eq. (8).

$$\varphi_L = \alpha_{Li} \frac{c_L}{1 - e^{-c_L}}(T_i - T_{Lb}) \tag{8}$$

with c being

$$c = \frac{\dot{m}_{NH_3} \tilde{c}_{p,NH_3} + \dot{m}_{H_2O} \tilde{c}_{p,H_2O}}{\alpha} \tag{9}$$

According to the control volume shown in Fig. 3, the energy balance at the liquid–vapour interface provides Eq. (10), which states the energy continuity and reflects the coupled heat and mass transfer nature at the interface.

$$\varphi_L = \varphi_v + \dot{m}_{NH_3} \Delta\tilde{h}_{NH_3} + \dot{m}_{H_2O} \Delta\tilde{h}_{H_2O} \tag{10}$$

where $\Delta\tilde{h}$ is the components' difference of vapour and liquid partial enthalpies at the interface conditions.

The heat flux transferred from the bulk liquid to the outer tube wall is given by Eq. (11).

$$\varphi_c = U_{\text{out}}(T_{\text{Lb}} - T_{\text{wo}}) \tag{11}$$

where

$$\frac{1}{U_{\text{out}}} = \frac{d_{\text{wo}}}{2k_w}\,\text{Ln}\left(\frac{d_{\text{wo}}}{d_{\text{wi}}}\right) + \frac{d_{\text{wo}}}{\alpha_{\text{Lw}} d_{\text{wi}}} \tag{12}$$

being α_{Lw} the heat transfer coefficient between the liquid phase and the inner tube wall.

The heat flux transferred from the outer tube wall to the coolant is given by Eq. (13)

$$\varphi_c = \frac{1}{1/\alpha_c + r_s}\Delta T_{\text{LM}} \tag{13}$$

where r_s is the coolant side fouling factor [39] and ΔT_{LM} is the logarithmic mean temperature difference, defined in Eq. (14).

$$\Delta T_{\text{LM}} = \frac{(T_{\text{wo}} - T_{\text{ci}}) - (T_{\text{wo}} - T_{\text{co}})}{\text{Ln}[\frac{T_{\text{wo}} - T_{\text{ci}}}{T_{\text{wo}} - T_{\text{co}}}]} \tag{14}$$

3.3. Mass and energy balances

Based on the differential control volume shown in Fig. 3; mass, concentration and energy balance equations are established.

$$\mathrm{d}\dot{M}_v = -\mathrm{d}\dot{M}_L \tag{15}$$

$$\mathrm{d}\big(\dot{M}_v x_v\big) = -\mathrm{d}\big(\dot{M}_L x_L\big) \tag{16}$$

$$\mathrm{d}\big(\dot{M}_v h_v\big) = -\mathrm{d}\big(\dot{M}_L h_L\big) - \varphi_c\,\mathrm{d}A_c \tag{17}$$

An analysis of the bulk vapour phase yields Eqs. (18)–(20).

$$\mathrm{d}\dot{M}_v = -\dot{m}\,\mathrm{d}A_i \tag{18}$$

$$\mathrm{d}\big(\dot{M}_v x_v\big) = -\dot{m}_{\text{NH}_3}\,\mathrm{d}A_i \tag{19}$$

$$\mathrm{d}\big(\dot{M}_v h_v\big) = -\big(\dot{m}_{\text{NH}_3}\tilde{h}_{v,\text{NH}_3} + \dot{m}_{\text{H}_2\text{O}}\tilde{h}_{v,\text{H}_2\text{O}} + \varphi_v\big)\,\mathrm{d}A_i \tag{20}$$

The heat and mass transfer area between the liquid and vapour phases $\mathrm{d}A_i$ is given in Eq. (21), where a_{esp} is the specific interfacial area. The heat transfer area from the tube wall to the coolant $\mathrm{d}A_c$, based on the outer tube diameter is calculated from Eq. (22).

$$\mathrm{d}A_i = a_{\text{esp}}\frac{\pi d_{\text{wi}}^2}{4}\mathrm{d}y \tag{21}$$

$$\mathrm{d}A_c = \pi d_{\text{wo}}\,\mathrm{d}y \tag{22}$$

Eqs. (1)–(22) constitute the mathematical model of the absorber, based on the assumed hypothesis.

3.4. Flow patterns and flow parameters

The hydrodynamics within the absorber is characterised by a changing two-phase flow, since the mass flow of vapour and liquid change continuously from the inlet conditions until the absorption process is completed. The heat and mass transfer coefficients, the specific interfacial area and the two-phase flow void fraction depend on the flow pattern. Thus, a detailed knowledge of the two-phase flow behaviour is required. In vertical tubular absorbers with co-currently upward flow inside the tubes, churn, slug and bubbly flow patterns are present, according to Infante Ferreira [17]. The three different regimes are depicted in Fig. 4(a).

The churn flow pattern is only an entrance effect just after the inlet nozzle [22] that causes an unstable flow region with a co-current upward flow of the liquid and vapour phases (see Fig. 4(b)). The churn flow regime can be studied under the annular flow model, as suggested by Ueda [40]. The interfacial radius r_i and the mean velocity in the liquid film, V_{Lf}, can be calculated iteratively from the Hikita and Ishimi [41] relations. The transition between churn flow and slug flow occurs when the entrance effects are dumped. Taitel et al. [22] and Hewitt and Roberts [23] developed two-phase flow regime maps for vertical tubes, but the predictions do not seem to be very realistic, as pointed out by Infante Ferreira [17] based on his experimental observations. These results highlight that the churn flow in the absorption process is only an entrance effect and the churning length should not be calculated from the two-phase flow regimen maps, because the churn flow conditions are not satisfied.

The slug flow pattern is characterised by the vapour phase rising as bullet shaped bubbles separated by slugs of liquid. The vapour bubbles almost fill the tube cross section and their length is large relative to the tube diameter. These long

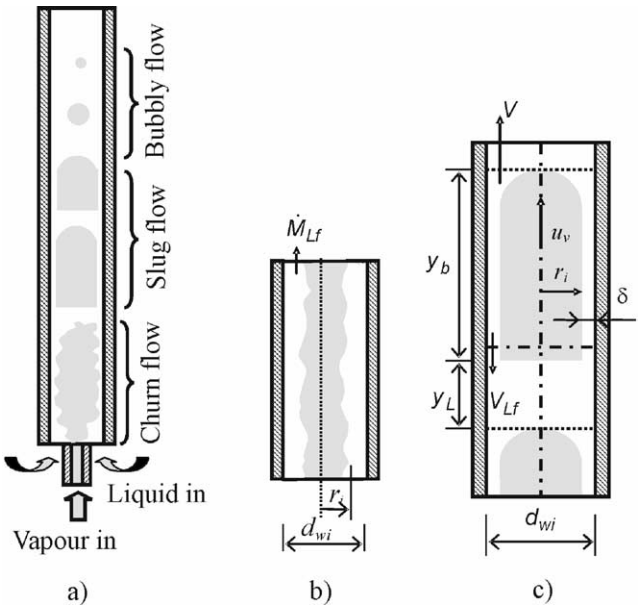

Fig. 4. Flow patterns in vertical tubular absorbers.

bubbles are known as Taylor bubbles [18]. In this paper it will be assumed that the Taylor bubble consists of a half sphere nose followed by a cylindrical body (see Fig. 4(c)) and it is surrounded by a thin liquid film. An iterative procedure must also be used to determine the interfacial radius r_i of the Taylor bubble and the mean velocity in the liquid film, V_{Lf}. By means of local material balance calculations, using Fig. 4(c), Eq. (23) can be written.

$$u_v r_i^2 - V\left(\frac{d_{\mathrm{wi}}}{2}\right)^2 = V_{\mathrm{Lf}}\left[\left(\frac{d_{\mathrm{wi}}}{2}\right)^2 - r_i^2\right] \tag{23}$$

where V is the total volume flux through the channel and u_v is the mean bubble rise velocity as proposed by Nicklin et al. [19] and Collins et al. [20]. V_{Lf} is the mean velocity in the film, which completes the iterative procedure using the Hikita and Ishimi [41] and Kriegel [42] correlations.

The bubble length y_b is given by Eq. (24).

$$y_b = \left[\frac{\dot{M}_v}{\rho_v \dot{N}_b} + \frac{1}{3}\pi r_i^2\right]\frac{1}{\pi r_i^2} \tag{24}$$

where $\dot{N}_b$ is the bubble frequency in the absorber. The separation distance, y_L, between two Taylor bubbles can be obtained from Eq. (25).

$$y_L = \frac{u_v}{\dot{N}_b} - y_b \tag{25}$$

The bubbly flow pattern is characterised by isolated spherical bubbles rising co-currently with the liquid [43]. This flow regimen arises at the end part of the absorption process.

The initial bubble size allows determining the bubble frequency in the absorber. Considering the churn flow only as an entrance effect, the initial bubble size will be obtained taking into account the slug flow and the Taylor bubble behaviour at the initial conditions. Pinto and Campos [14] and Pinto et al. [15] obtained the minimum slug length of a liquid plug where the slug flow regime remains stable. Following Pinto et al. [15] it will be assumed that the minimum slug length is ($y_{\mathrm{Lmin}} = 5d_{\mathrm{wi}}$), and this length will be taken as the initial slug length (y_L). The Taylor bubble length, the initial bubble volume and the bubble frequency are calculated iteratively by means of Eqs. (24) and (25). The two-phase flow void fraction is obtained from Nicklin et al. [19] in churn and slug flows and from Zuber and Findlay [44] in bubbly flow. Both methods are based on the drift flux model [45]. The specific interfacial area in churn and in slug flow is calculated as the surface area of the bubble per unit liquid–vapour volume [36]. In bubbly flow the correlation proposed by Hikita et al. [46] is used.

In this paper, the churn flow region length is considered to be equal to the initial bubble length, because the churn flow exists while the vapour is coming into the tube. After the vapour bubble detaches from the nozzle it will evolve into the slug flow pattern. The slug to bubbly flow pattern transition occurs for a slug bubble length less than the inner tube radius (Moissis [24]).

3.5. Heat and mass transfer coefficients

In churn and slug flows, the heat transfer coefficient in the vapour phase (α_v) is obtained from Gnielinski [47]. The heat transfer coefficient between the liquid and the liquid–vapour interface (α_{Li}) is calculated from the film wise condensation theory [48–50], as pointed out by Kim et al. [33]. In bubbly flow, the vapour phase heat transfer coefficient (α_v) is calculated by means of the Chilton and Colburn analogy [51] from the mass transfer coefficient (F_v). The heat transfer coefficient in the liquid phase (α_{Li}) is obtained from Deckwer [25].

In churn and slug flows, the vapour phase mass transfer coefficient (F_v) is obtained by using the Chilton and Colburn analogy from the heat transfer coefficient (α_v). In bubbly flow, the correlation proposed by Clift et al. [52] is used. In churn flow, the mass transfer coefficient between the liquid phase and the liquid–vapour interface (F_{Li}) is obtained using the Chilton and Colburn analogy from the heat transfer coefficient (α_{Li}). In slug flow, the correlation proposed by Lamourelle and Sandall [26] is applied. In bubbly flow the equation proposed by Hughmark [27] for isolated bubbles is used.

In churn flow, the heat transfer coefficient between the liquid phase and the tube wall (α_{Lw}) is considered to be equal to the heat transfer coefficient between the liquid phase and the liquid–vapour interface (α_{Li}). In slug and bubbly flows, the heat transfer coefficient between the liquid phase and the tube wall (α_{Lw}) is calculated weighing up the heat transfer coefficient in the liquid (α_{Li}) and the single-phase heat transfer coefficient (α_{Lsp}) obtained from Gnielinski [47] for turbulent flow and from Kays and Crawford [53] for laminar flow, using the formula proposed by Keizer [54] (Eq. (26)). The heat transfer coefficient between the tube wall and the coolant (α_c) is obtained from Zukauskas et al. [55].

$$\alpha_{\mathrm{Lw}} = \varepsilon_v \alpha_{\mathrm{Li}} + (1 - \varepsilon_v)\alpha_{\mathrm{Lsp}} \tag{26}$$

4. Solution method

The previous set of non-linear differential equations cannot be solved analytically; therefore a finite-difference numerical method has been used. The absorber length at each between-baffles section has been divided in a finite number of elements n_{sb} with an incremental length Δy.

The coolant is introduced at the top of the absorber driven by the baffles and heated up when it contacts the tube bundle. If inlet coolant, liquid and vapour conditions were known at any incremental element ($i = 1, \ldots, n$), then the outlet conditions would be obtained. Since heat and mass transfer processes should be considered simultaneously in order to obtain the unknown conditions, heat and mass transfer equations and mass, concentration and energy balances should be solved together. As shown in Eqs. (2) and (3), mass transfer

depends on the value of ratio z and the interface temperature. On the other hand, the heat transferred between the vapour and liquid phases given by Eq. (10) depends on the interface temperature T_i and the ammonia and total mass transferred. Moreover, the heat flux transferred between the bulk liquid and the coolant, shown in Eqs. (11) and (12), depends on the outer tube wall temperature T_{wo} and the logarithmic mean temperature difference with the coolant. Taking all these things into account, an iterative procedure must be implemented to solve the finite difference equations obtained from the discretization of Eqs. (1)–(22).

The following algorithm uses four iterative loops to obtain the values of the ratio z, the interface temperature T_i, the outer tube wall temperature T_{wo} and the coolant outlet temperature T_{co}. Once these parameters are calculated, the vapour and liquid conditions of the next incremental element can be obtained. The calculation procedure is summarised below.

(1) Guess the interface temperature T_i.
(2) Calculate $\bar{x}_{Li}$ and $\bar{x}_{vi}$ with the assumed interface temperature and the absorber pressure, considering equilibrium and saturation conditions.
(3) Guess z.
(4) Calculate $\dot{n}_{NH_3}|_v$ and $\dot{n}_{NH_3}|_L$ from Eqs. (2) and (3).
(5) If $\dot{n}_{NH_3}|_v = \dot{n}_{NH_3}|_L$, go to step 6, otherwise guess a new value of z and go to step 4.
(6) Calculate the sensible heat transferred from vapour and liquid phases, using Eqs. (7) and (8).
(7) Check the energy balance at the interface using Eq. (10). If verified, go to step 8, otherwise guess a new value of T_i and go to step 2.
(8) Calculate the ammonia and total mass fluxes transferred from Eqs. (5) and (6).
(9) Guess T_{wo}.
(10) Calculate the heat flux transferred from the bulk liquid to the outer tube wall from Eq. (11).
(11) Guess T_{co}.
(12) Calculate the heat flux transferred from the outer tube wall to the coolant, using Eqs. (13) and (14).
(13) Check T_{co} using Eq. (27). If the values are equal go to step 14, otherwise guess a new T_{co} and go to step 12.

$$T_{co} = T_{ci} + \frac{\varphi_c \Delta A_c}{\frac{\dot{M}_c}{n_{sb}} c_{p,H_2O}} \tag{27}$$

(14) Check the heat fluxes obtained in steps 10 and 12. If they are equal go to step 15, otherwise guess a new T_{wo} and go to step 10.
(15) The new vapour and liquid conditions can now be obtained from Eqs. (15)–(20).

Once the previous algorithm is applied to the n_{sb} elements of any between-baffles section (j) an outlet coolant temperature profile is obtained.

The coolant mixes while flowing down to the adjoining between-baffles section. Therefore, the coolant temperature at the inlet of the $(j-1)$ between-baffles section is considered to be equal to the coolant average temperature at the outlet of the j-section, according to Eq. (28) and assuming the coolant specific heat is constant.

$$T_{ci}(j-1) = \frac{\sum_{i=n_{sb}(j-1)+1}^{n_{sb}\,j} T_{co}(i)}{n_{sb}}, \quad j = 2, \ldots, N_b + 1 \tag{28}$$

where the inlet coolant temperature at each i-element is obtained from Eq. (29).

$$T_{ci}(i) = T_{ci}(j-1), \quad i = n_{sb}(j-2)+1, \ldots, n_{sb}(j-1) \tag{29}$$

The absorber is solved from the bottom to the top. The vapour and the weak solution conditions are known at the bottom and the cooling water temperature at the top. Therefore, the inlet coolant temperature $T_{ci}(j)$ for each (j) between-baffles section must be assumed. Then, the outlet coolant temperatures (T_{co}) are obtained and a trial and error method is applied until Eq. (28) is verified with the inlet coolant temperature $T_{ci}(j-1)$ from the previous between-baffles section. This procedure must be carried out along the absorber.

The solution method explained above has been implemented in a computer program using FORTRAN 95. State equations required for NH_3–H_2O equilibrium and thermodynamic properties are taken from Ziegler and Trepp [56].

5. Results and discussion

The initial data required by the computer program are the absorber geometry and material thermal properties, as well as the absorber operating conditions. The results provided by the program are the distributions along the tubes length of several parameters such as: temperature, concentration and mass flow of the vapour and liquid phases, interface temperature and interface liquid and vapour concentrations, the coolant and tube wall temperatures; the ammonia, water and total molar fluxes transferred between phases, the ratio z of ammonia to total molar flux, the heat and mass transfer coefficients, the void fraction, the bubble volume, the specific interfacial area and the heat transfer fluxes. The program was used to simulate and analyse the performance of tubular vertical absorbers considering data from different practical applications. Furthermore, a parametric study was carried out in order to analyse the influence of each design parameter and operating condition on the absorber performance. Results for a specific application are presented here.

The geometry and material thermal properties of the absorber are specified in Table 1. The operating conditions are shown in Table 2. These data characterise representative design and operating conditions of an absorber for a small capacity ammonia–water absorption refrigeration system [57]. Direct numerical results are shown in Table 3. The different

Table 1
Geometry and material thermal properties of the absorber

Absorber length [m]	0.9
Inner tube diameter [m]	0.022
Outer tube diameter [m]	0.025
Number of baffles	12
Number of tubes	40
Nozzle diameter [m]	0.009
Thermal conductivity [$W \cdot m^{-1} \cdot K^{-1}$]	13
Coolant side fouling factor [$m^2 \cdot K \cdot kW^{-1}$]	0.2

Table 2
Absorber operating conditions

Vapour mass flow rate [$kg \cdot h^{-1}$]	15.0
Vapour concentration [kg $NH_3 \cdot kg^{-1}$]	0.999
Vapour temperature [K]	283.15
Inner tube pressure [bar]	2.0
Weak solution mass flow rate [$kg \cdot h^{-1}$]	100.0
Weak solution concentration [kg $NH_3 \cdot kg^{-1}$]	0.225
Weak solution temperature [K]	318.15
Coolant mass flow rate [$kg \cdot h^{-1}$]	1500.0
Coolant temperature [K]	293.15

Table 3
Results

Strong solution mass flow rate [$kg \cdot h^{-1}$]	115.0
Strong solution concentration [kg $NH_3 \cdot kg^{-1}$]	0.324
Strong solution temperature [K]	298.23
Coolant outlet temperature [K]	298.78
Absorption length [m]	0.783

parameter distributions along the absorber tubes length are shown in the next figures.

Fig. 5 shows the vapour mass flow rate along the length of the absorber tubes. The horizontal dashed lines on the figure point out the transition between flow patterns (churn to slug and slug to bubbly flows) and the absorption achievement. The vapour mass flow is the most representative variable to characterize the absorber performance, since the evolution of the absorption process can be easily followed on the figure. The absorption is considered completed when the vapour mass flow is less than 1% of its initial value. The length from the bottom to the point where the absorption process is completed is named as the absorption length. From the absorption length to the top of the tubes only single liquid phase flow exists. The dissimilar absorption rates within the tubes for the different flow patterns can be observed.

Fig. 6 depicts temperature profiles along the absorber length. The horizontal dashed lines point out the transition between flow patterns and the absorption length. The discontinuities in temperatures when the transition between two different flow regimes takes place are due to different heat and mass transfer correlations. It can be seen that the vapour (T_{vb}) and interface (T_i) temperature distributions come to an end on the absorption length. In the churn flow region the liquid (T_{Lb}) temperature decreases. However, at the beginning of the slug flow zone a slight increase in the liquid

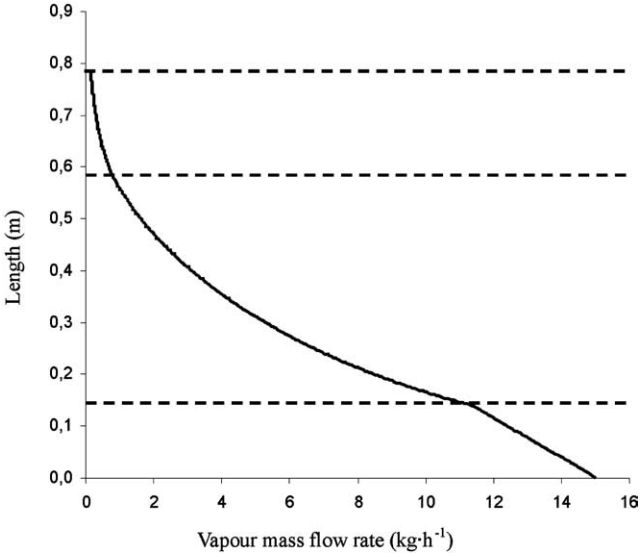

Fig. 5. Vapour mass flow rate profile along the absorber length.

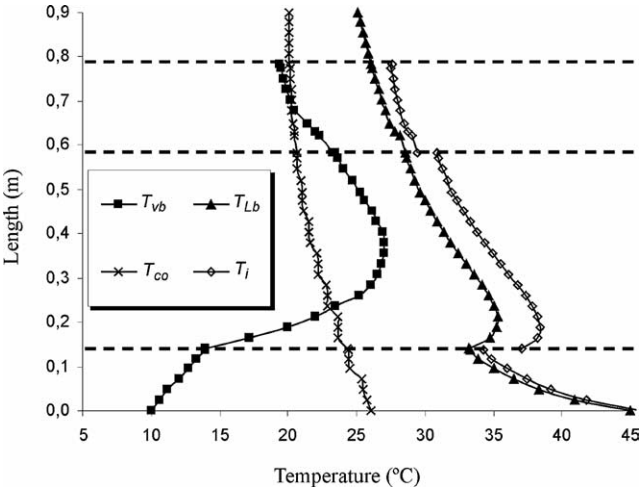

Fig. 6. Temperature profiles along the absorber length.

(T_{Lb}) temperature is observed, as a consequence of high mass and heat transfer rates at this absorption stage. Further in the absorber, the liquid temperature drops again up to the top of the absorber length. The inlet vapour (T_{vb}) temperature is much lower than the liquid (T_{Lb}) and interface (T_i) temperatures, rising quickly when churn and slug regimens take place in the tubes. At the end of slug flow and in the bubbly flow regime the vapour temperature (T_{vb}) decreases, moving away from both the interface and liquid temperatures. The liquid and vapour temperatures are always lower than the interface temperature. However, the liquid temperature (T_{Lb}) is closer to the interface (T_i) temperature than the vapour (T_{vb}) temperature. This denotes that the heat transfer resistance is dominant in the vapour rather than in the liquid phase. The cooling water (T_{co}) temperature profile is also plotted in Fig. 6. The coolant circulates counter-current to the two-phase flow inside the tubes. The temperature distribution spreads out at intervals due to the baffles mixing

effect. The water temperature increases from the top to the bottom of the absorber. However, the increase of the coolant temperature at the lower part of the absorber is more significant than at the upper zone because the heat generated by the absorption process is higher.

Fig. 7 shows the interface and bulk liquid ammonia molar concentrations along the absorber tubes length. The bulk liquid concentration ($\bar{x}_{\mathrm{Lb}}$) increases throughout the absorption length and remains constant up to the tube top. It can be seen that the bulk liquid concentration ($\bar{x}_{\mathrm{Lb}}$) enlargement is larger in churn and slug flows than in bubbly flow. The interface liquid concentration ($\bar{x}_{\mathrm{Li}}$) remains always higher than the bulk liquid concentration.

The profiles of the vapour molar concentrations at the bulk ($\bar{x}_{\mathrm{vb}}$) and at the interface ($\bar{x}_{\mathrm{vi}}$) as well as the ratio of ammonia molar flux to the total molar flux transferred (z) are depicted in Fig. 8. The vapour and liquid concentrations at the interface evolve in the same way, as can be seen from Figs. 7 and 8. The bulk vapour concentration ($\bar{x}_{\mathrm{vb}}$) decreases in the churn flow region and in the slug region while the bulk concentration ($\bar{x}_{\mathrm{vb}}$) is greater than the interface concentration ($\bar{x}_{\mathrm{vi}}$). Once the bulk vapour concentration line crosses the curve of the interface concentration and the bulk concentration becomes smaller than the interface concentration, the bulk vapour concentration increases slowly until the end of the absorption process is attained.

The ratio of ammonia molar flux to the total molar flux (z) is greater than the vapour concentrations up to the point where the three magnitudes become equal. Afterwards, z becomes lower than the vapour concentrations. However, z remains always higher than the interface liquid concentration ($\bar{x}_{\mathrm{Li}}$), as can be seen in Fig. 7. Therefore the total molar flux and the ammonia molar flux are always from the vapour to the liquid phase, according to Eqs. (1)–(3). In the churn flow region and in the slug region up to the length of 24.4 cm, the ratio of ammonia molar flux to the total molar flux (z) is greater than 1. Therefore ammonia is absorbed from the vapour into the liquid and water is desorbed into the vapour region according to Eq. (2). From the length of 24.4 cm up to the end of absorption process, the z values are smaller than 1, therefore both ammonia and water components are absorbed from the vapour phase into the liquid phase. The phenomenon of initial water desorption in the ammonia–water absorption process has been also reported by Herbine and Perez-Blanco [10] for a co-current ammonia–water bubble absorber and by Kang et al. [7,13] for a counter-current ammonia–water bubble absorber.

Parametric analysis was carried out in order to evaluate the influence of the geometrical design parameters and the operating conditions on the absorber design and performance. Each parameter was varied while keeping all other constant and equal to the data given in Tables 1 and 2. The effect of each parameter was evaluated by considering its influence on the tubes length required for the complete absorption achievement.

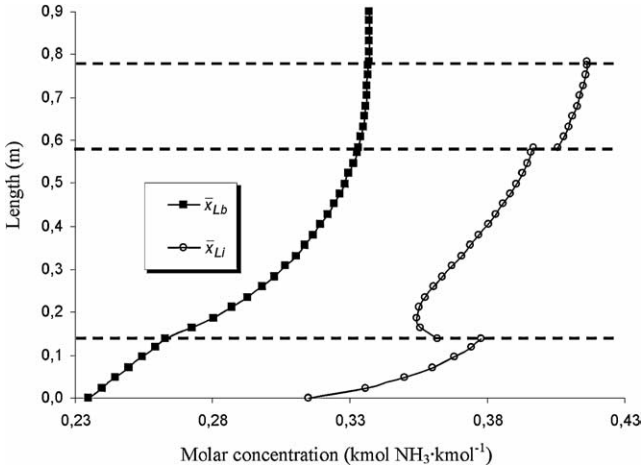

Fig. 7. Liquid phase molar ammonia concentrations profiles along the absorber length.

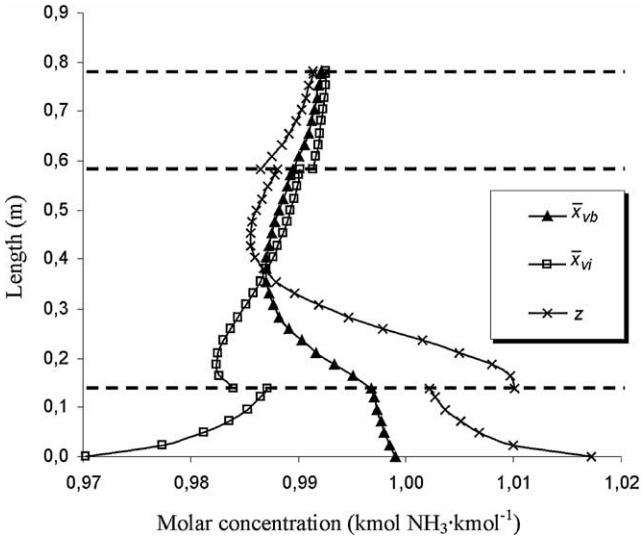

Fig. 8. Vapour phase molar ammonia concentrations and ratio z profiles along the absorber length.

The effect of the inner tube diameter on the required tubes length for the complete absorption achievement is illustrated in Fig. 9. The diameter and length of the tubes are the key parameters from the standpoint of the absorber design. Therefore the results presented in Fig. 9 can be very helpful. These results state the decisive influence of the tubes diameter on the required absorption length and consequently on the absorber size. It is noteworthy the sharply impact of the tube diameter on the absorption length for diameter values lower than 30 mm and in particular for diameters lower than 20 mm, as it can be seen in the figure. Moreover, it is also noticeable the small influence of tube diameter for values greater than 30 mm on the absorption length. Furthermore, the results in Fig. 9 also reveal the existence of an optimal tubes diameter, which leads to complete the absorption process with the shortest tubes length. The existence of an optimal inner diameter is a consequence of a balance between longer slug flow pattern regions (where the liquid heat

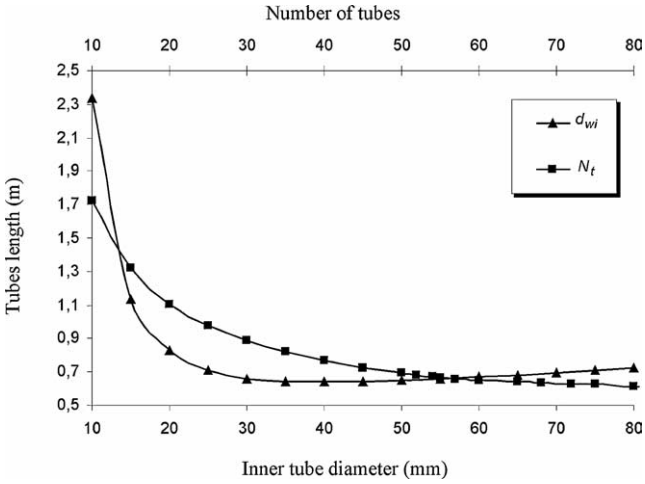

Fig. 9. The effect of inner tube diameter and number of tubes on the required tubes length for the absorption process completion.

and mass transfer coefficients are higher than in bubbly flow) and the decrease of bubble frequency (which leads to bigger bubbles) and the reduction of the transfer area with the reduction of the inner tube diameter. With the data considered in the analysis, the minimum absorption length corresponds to tubes with 35 mm inner diameter. It has been also found that with inner tube diameters bigger than 70 mm only bubbly flow takes place in the tubes.

Fig. 9 also shows the influence of the number of tubes in the absorber on the tubes length required for the absorption completion. The required tubes length decreases when the number of tubes increases, as it is concluded from the results shown in the figure. However, it is noticeable that the reduction attainable in the required tubes length diminishes as the number of tubes increases. It should be pointed that in Fig. 9 a perfect continuous trend is not obtained when varying the number of tubes because this variation is discrete and the tube bank configuration is also affected.

Fig. 10 shows the evolution of the required tubes length for the absorption completion when varying the weak solution concentration and the inlet cooling water temperature. The results show that the tubes length increases considerably with the weak solution concentration. Low weak solution concentrations reduce the required tubes length by promoting the mass transfer process. Experimental results obtained by Kim et al. [32] agree with the results reported in the figure. For the data considered in this application (Tables 1 and 2) the strong solution saturation temperature results 41.7 °C. This temperature constitutes the limit for the coolant inlet temperature. The results in the figure reflect that the required tubes length increases with the coolant temperature. This trend is strengthened as the coolant temperature approaches to the strong solution saturation temperature; however, when reducing the cooling water temperature this variable is not a limiting one and its effect on the required tubes length is weaker.

Fig. 11 shows the influence of the heat transfer coefficients in the liquid (α_{Li}), vapour (α_v), and in the coolant (α_c)

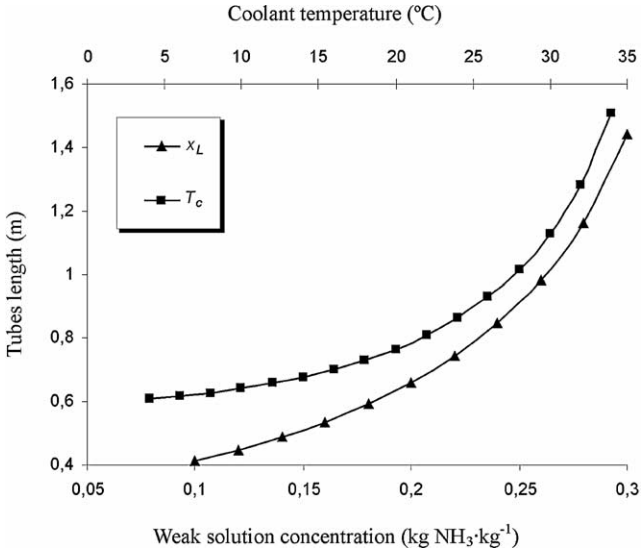

Fig. 10. The effect of the weak solution ammonia concentration and the coolant temperature on the required tubes length for the absorption process completion.

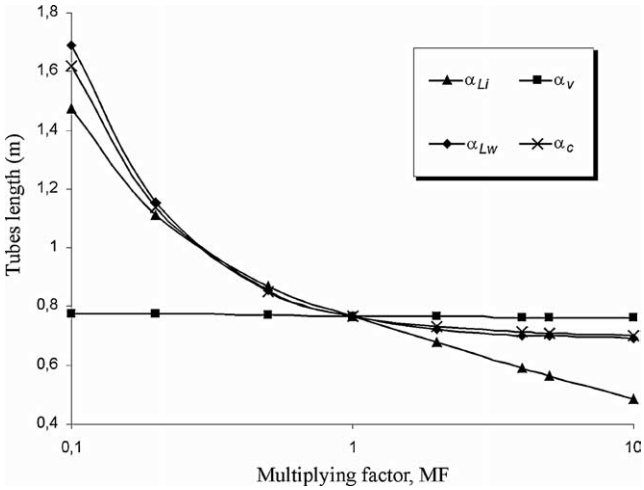

Fig. 11. The effect of heat transfer coefficients on the required tubes length for the absorption process completion.

regions as well as between the liquid and tube wall (α_{Lw}), on the required tubes length for the absorption completion. The heat transfer coefficient between the liquid and the liquid–vapour interface (α_{Li}) has the most significant effect on the tubes length. The heat transfer coefficient between the liquid and the tube wall (α_{Lw}) is the next more important factor, followed by the heat transfer coefficient in the coolant (α_c). The heat transfer coefficient in the vapour phase has no significant effect on the absorber length beyond a multiplying factor (MF) of 0.5. The influence of the mass transfer coefficients in the liquid (F_{Li}) and the vapour (F_v) regions on the required tubes length is shown in Fig. 12. The mass transfer coefficient in the liquid phase has a more important effect on the tubes length than the mass transfer coefficient in the vapour phase. Kang et al. [7,13] also obtained similar results for the counter-current bubble absorber.

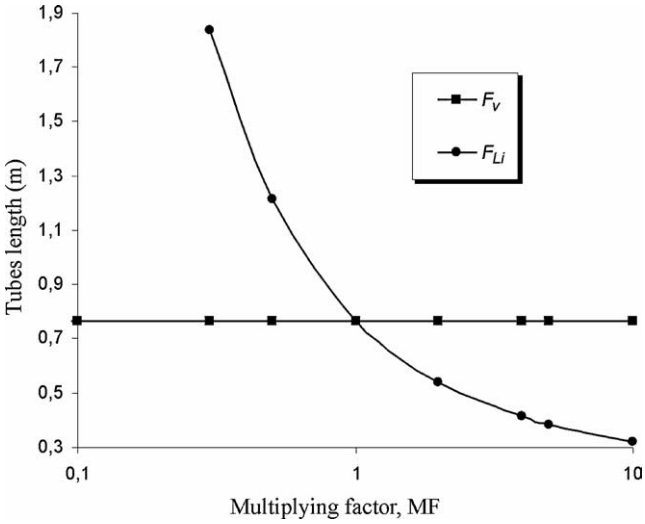

Fig. 12. The effect of mass transfer coefficients on the required tubes length for the absorption process completion.

6. Conclusions

In this paper, a detailed analysis of the heat and mass transfer processes during the absorption of ammonia into water in a co-current vertical tubular absorber has been presented. The analysis has been carried out developing a differential mathematical model based on mass and energy balances and the heat and mass transfer equations. The model takes into account separately the churn, slug and bubbly flow patterns experimentally forecasted in this type of absorbers process.

The results show that the absorption process progresses rapidly in the churn and in the slug flow regions but slows down in the bubbly flow. The interface temperature is nearly equal to the bulk liquid temperature; therefore the heat transfer resistance is located mainly in the vapour phase. The results also predict water desorption at the beginning of the absorption process.

The diameter and length of the tubes are the key parameters from the standpoint of the absorber design. The results reveal the existence of an optimal inner tube diameter that minimises the required tubes length. For tube diameters lower than the optimal diameter the influence on the tubes length is very significant. The increase in the number of tubes causes the reduction of the required tubes length; however, the reduction attainable diminishes as the number of tubes increases. Low weak solution concentrations reduce the required tubes length by promoting the mass transfer process. The tubes length increases with the coolant temperature and this trend is strengthened as the coolant temperature approaches to the strong solution saturation temperature. The heat and mass transfer coefficients in the vapour phase have no significant effect on the absorption process. However, the others heat and mass transfer coefficients should be always taken into account in the analysis, since their effects on the absorption process are important.

References

[1] J. Fernández-Seara, A. Vales, M. Vázquez, Heat recovery system to power an onboard NH_3–H_2O absorption refrigeration plant in trawler chiller fishing vessels, Appl. Therm. Engrg. 18 (1998) 1189–1205.
[2] F. Ziegler, Recent developments and future prospects of obsorption heat pump systems, Internat. J. Therm. Sci. 38 (1999) 191–208.
[3] K.E. Herold, R. Radermacher, S.A. Kelin, Absorption Chillers and Heat Pumps, CRC Press, New York, 1996.
[4] J. Fernández-Seara, J. Sieres, M. Vázquez, Simultaneous heat and mass transfer of a packed distillation column for ammonia–water absorption refrigeration systems, Internat. J. Therm. Sci. 41 (2002) 927–935.
[5] J. Fernández-Seara, J. Sieres, M. Vázquez, Distillation column configurations in ammonia–water absorption refrigeration systems, Internat. J. Refrig. 26 (2003) 28–34.
[6] J. Fernández-Seara, J. Sieres, M. Vázquez, Heat and mass transfer analysis of a helical coil rectifier in an ammonia–water absorption system, Internat. J. Therm. Sci. 42 (2003) 783–794.
[7] Y.T. Kang, R.N. Christensen, T. Kashiwagi, Ammonia–water bubble absorber with a plate heat exchanger, ASHRAE Trans. 104 (1998) 956–966.
[8] C.A. Infante Ferreira, C. Keizer, C.M.M. Machielsen, Heat and mass transfer in vertical tubular bubble absorbers for ammonia–water absorption refrigeration systems, Internat. J. Refrig. 7 (1984) 348–357.
[9] T.L. Merril, H. Setoguchi, Pérez-Blanco Compact bubble absorber design and analysis, International Absorption Heat Pump Conference, ASME, New Orleans, January, 1994.
[10] G.S. Herbine, H. Pérez-Blanco, Model of an ammonia–water bubble absorber, ASHRAE Technical Data Bull. 11 (1995) 102–110.
[11] S.V. Potnis, A. Gomezplata, R.A. Papar, G. Anand, D.C. Erickson, GAX component simulation and validation, ASHRAE Trans. 103 (1997).
[12] A.P. Colburn, T.B. Drew, The condensation of mixed vapours, AIChE Trans. 33 (1937) 197–215.
[13] Y.T. Kang, A. Akisawa, T. Kashiwagi, Analytical investigation of two different absorption modes: falling film and bubble types, Internat. J. Refrig. 23 (2000) 430–443.
[14] A.M.F.R. Pinto, Campos J.B.L.M. Coalescence of two gas slugs rising in a vertical column of liquid, Chem. Engrg. Sci. 51 (1996) 45–54.
[15] A.M.F.R. Pinto, M.N. Coelho Pinheiro, J.B.L.M. Campos, Coalescence of two gas slugs rising in a co-current flowing liquid in vertical tubes, Chem. Engrg. Sci. 53 (1998) 2973–2983.
[16] Jr.J.R. Barbosa, A.H. Govan, G.F. Hewitt, Visualisation and modelling studies of churn flow in a vertical pipe, Internat. J. Multiphase Flow 27 (2001) 2105–2127.
[17] C.A. Infante Ferreira, Vertical tubular absorbers for ammonia-salt absorption refrigeration, Ph.D. Thesis, Delft University of Technology, Netherlands, 1985.
[18] P. Griffith, G.B. Wallis, Two-phase slug flow, ASME J. Heat Transfer 83 (1961) 307–320.
[19] D.J. Nicklin, J.O. Wilkes, J.F. Davidson, Two-phase flow in vertical tubes, Trans. Inst. Chem. Engrg. 40 (1962) 61–68.
[20] R. Collins, F.F. De Moraes, J.F. Davidson, D. Harrison, The motion of large gas bubble rising through liquid flowing in a tube, J. Fluid Mech. 89 (1978) 497–514.
[21] X.T. Chen, J.P. Brill, Slug to churn transition in upward vertical two-phase flow, Chem. Engrg. Sci. 52 (1997) 4269–4272.
[22] Y. Taitel, D. Bornea, A.E. Dukler, Modelling flow pattern transitions for steady upward gas-liquid flow in vertical tubes, AIChE J. 26 (1980) 345–354.
[23] G.F. Hewitt, D.N. Roberts, Studies of two-phase flow patterns by simultaneous X-ray and flash photography AEREM2159, 1969.
[24] R. Moissis, The transition from slug to homogeneous two-phase flows, Trans. ASME J. Heat Transfer C 85 (1963) 366–370.
[25] W.D. Deckwer, On the mechanism of heat transfer in bubble column reactors, Chem. Engrg. Sci. 35 (1980) 1341–1349.

[26] A.P. Lamourelle, O.C. Sandall, Gas absorption into a turbulent liquid, Chem. Engrg. Sci. 27 (1972) 1035–1043.
[27] G.A. Hughmark, Holdup and mass transfer in bubble columns, Indust. Engrg. Chem. Proc. Des. Dev. 6 (1967) 218–220.
[28] T. Elperin, A. Fominykh, Four stages of the simultaneous mass and heat transfer during bubble formation and rise in bubbly absorber, Chem. Engrg. Sci. 58 (2003) 3555–3564.
[29] K. Teresaka, J. Oka, H. Tsuge, Ammonia absorption from a bubble expanding at a submerged orifice into water, Chem. Engrg. Sci. 57 (2002) 3757–3765.
[30] Y.T. Kang, T. Nagano, T. Kashiwagi, Mass transfer correlation of NH_3–H_2O bubble absorption, Internat. J. Refrig. 25 (2002) 878–886.
[31] J. Lee, K. Lee, B. Chun, C. Lee, J. Joo Ha, S.H. Kim, A study on numerical simulations and experiments for mass transfer in bubble mode absorber of ammonia and water, Internat. J. Refrig. 26 (2003) 551–558.
[32] H.Y. Kim, B.B. Saha, S. Koyama, Development of a slug flow absorber working with ammonia–water mixture: Part I—Flow characterization and experimental investigation, Internat. J. Refrig. 26 (2003) 508–515.
[33] H.Y. Kim, B.B. Saha, S. Koyama, Development of a slug flow absorber working with ammonia–water mixture: Part II—Data reduction model for local heat and mass transfer characterization, Internat. J. Refrig. 26 (2003) 698–706.
[34] W.K. Lewis, W.G. Whitman, Principles of gas absorption, Indust. Engrg. Chem. 16 (1924) 1215–1220.
[35] R.B. Bird, W.E. Steward, E.N. Lightfoot, Transport Phenomena, Wiley, New York, 1960.
[36] R.E. Treybal, Mass Transfer Operations, McGraw-Hill, New York, 1980.
[37] D.R. Webb, The condensation of vapour mixtures, in: Heat Exchanger Design Handbook, Begell House, 1998.
[38] T.K. Sherwood, R.L. Pigford, C.R. Wilke, Mass Transfer, McGraw-Hill, New York, 1975.
[39] J.G. Knudsen, Recommended fouling resistances for design, in: Heat Exchanger Design Handbook, Begell House, 1998.
[40] T. Ueda, On upward flow of gas–liquid mixtures in vertical tubes, 2nd report, consideration of frictional pressure drop and void fraction, Bull. JSME 10 (1967) 1000–1007.
[41] H. Hikita, K. Ishimi, Frictional pressure drop for laminar gas streams in whetted-wall columns with co-current and counter-current gas–liquid flow, J. Chem. Engrg. Japan 9 (1976) 357–362.
[42] E. Kriegel, Berechnung von zweiphasenströmungen von gas/flüs sigkeits-systemen in rohren, Chemie Ing. Techn. 39 (1967) 1267–1274.
[43] G.F. Hewitt, Gas–liquid flow, in: Heat Exchanger Design Handbook, Begell House, 1998.
[44] N. Zuber, J.A. Findlay, Average volumetric concentration in two-phase flow systems, Trans. ASME J. Heat Transfer 87 (1965) 453–468.
[45] G.B. Wallis, One-Dimensional Two-Phase Flow, McGraw-Hill, New York, 1969.
[46] H.S. Hikita, K. Tanigawa, K. Segawa, M. Kitao, Gas hold-up in bubble column, Chem. Engrg. J. 20 (1980) 59–65.
[47] V. Gnielinski, New equations for heat and mass transfer in turbulent pipe and channel flow, Internat. Chem. Engrg. 15 (1976) 356–368.
[48] W. Nusselt, Die oberflachenkondensation des wasserdampfes, Z. Ver. Deut. Ing. 60 (1916) 541.
[49] S.S. Kutateladze, Fundamentals of Heat Transfer, Academic Press, New York, 1963.
[50] J.M. McNaught, D. Butterworth, Film condensation of pure vapour, in: Heat Exchanger Design Handbook, Begell House, 1998.
[51] T.H. Chilton, A.P. Colburn, Mass transfer (absorption) coefficients, Indust. Engrg. Chem. 26 (1934) 1183–1187.
[52] R. Clift, J.R. Grace, M.E. Weber, Bubbles, Drops and Particles, Academic Press, New York, 1978.
[53] W.M. Kays, M.E. Crawford, Convective Heat and Mass Transfer, McGraw-Hill, New York, 1980.
[54] C. Keizer, Absorption refrigeration machines, Ph.D. Thesis, Delft University of Technology, Netherlands, 1982.
[55] A. Zukauskas, V. Makarevicius, A.S. Slanciauskas, Heat Transfer in Banks of Tubes in Crossflow of Fluid, Mintis, Vilnius, 1968.
[56] B. Ziegler, Ch. Trepp, Equation of state of ammonia–water mixtures, Internat. J. Refrig. 7 (1984) 101–106.
[57] J. Fernández-Seara, J. Sieres, M. Vázquez, Absorption refrigeration prototype for onboard cooling production in fishing vessels, in: R. Wang, Z. Lu, W. Wang, X. Huang (Eds.), Proceedings of the International Sorption Heat Pump Conference, ISHPC2002, Science Press, Shanghai, China, 2002, pp. 130–135.